Selective Activation of GPCRs: Molecular Dynamics Investigation of Siponimod's Interaction with S1PR1 and S1PR2

Kumari Soniya,[1] Chanukya Nanduru,[1] and Antarip Halder[1]
[1]*Aganitha, 512T, Road number 29, Jubilee Hills, Hyderabad, Telangana-500033, India*

(*Electronic mail: soniya@aganitha.ai)

(Dated: 9 July 2024)

Understanding drug selectivity is crucial for designing effective medications that target specific proteins while minimizing off-target interactions, thus optimizing therapeutic outcomes. Although biochemical and cellular assays provide valuable insights on functional characterization, they offer limited understanding on molecular details of selectivity, particularly for targets within large families of structurally and functionally similar proteins. In such situations, carefully designed computational studies can complement experimental approaches, bridging gaps and deepening our understanding of drug selectivity mechanisms. In this study, Molecular Dynamics (MD) simulations along with structural bioinformatics methods have been used to examine the selectivity of Siponimod, an FDA-approved drug, towards sphingosine-1-phosphate receptor 1 (S1PR1) to treat Multiple Sclerosis (MS). Specifically, we investigated why Siponimod activates S1PR1 but not S1PR2, even though both receptors belong to the same sub-family of G Protein-Coupled Receptors (GPCRs). Contrary to the previous hypothesis based on molecular docking, MD simulations showed that Siponimod can bind to S1PR2 with an *in silico*-determined affinity comparable to that of S1PR1. Comparing the dynamics of Siponimod-bound S1PR2 with S1P-bound S1PR2 revealed that the transmission switches necessary for downstream biological activity are activated by S1P but not by Siponimod. Whereas, both S1P and Siponimod activate those transmission switches in S1PR1. A few crucial residues in S1PR2 were also identified that can be leveraged to optimize molecules to bind selectively to S1PR1 over S1PR2. Through our study, we showed that *in silico* approaches can help in understanding the ligand induced structural changes and aid in developing and optimizing drugs for GPCRs, the most abundant class of membrane proteins in the human genome and the largest family of membrane receptors targeted by approved drugs.

I. INTRODUCTION

G protein-coupled receptors (GPCRs) constitute the most prevalent class of integral membrane proteins encoded in the human genome[1]. Additionally, they comprise the largest family of membrane receptors that are the focus of approved pharmaceutical interventions[2]. However, designing a drug targeting GPCRs is challenging due to the high sequence and structural homology among members of the same sub-family, making it difficult to achieve selectivity. This similarity increases the risk of off-target effects, necessitating precise molecular design to differentiate between closely related receptors[3,4].

Among ∼800 GPCRs encoded in the human genome, five class A GPCRs are highly specific for sphingosine-1-phosphate (S1P) binding[5]. These are known as S1P receptors (S1PR1 through S1PR5). S1P, a signaling lysophospholipid, is produced by the phosphorylation of sphingosine via either sphingosine kinase 1 or sphingosine kinase 2[6]. The S1P gradient regulates immune cell traffic between lymphoid organs and circulation through S1PR1[7]. When S1PR1 binds to S1P, it undergoes internalization, reducing receptor presence on the cell surface and preventing lymphocytes from sensing the S1P gradient. As a result, lymphocytes are confined within lymphoid tissues[8,9]. This mechanism makes S1PR1 a valuable target for treating autoimmune diseases such as Multiple Sclerosis (MS)[10–12], tackling transplant rejections, and addressing conditions like Pulmonary Fibrosis[11,13,14]. The receptor subtypes S1PR1, S1PR2 and S1PR3 are primarily expressed in the cardiovascular, central nervous, and immune systems, whereas the expression of S1PR4 and S1PR5 is restricted to the immune and nervous systems[15,16]. S1PR2 is also linked with deafness in mice if the gene is mutated or knocked out.[17,18]

Certainly, while designing drugs for S1PR1, it is ideal to ensure that the drugs do not modulate other receptors, specifically S1PR2 and S1PR3 due to their involvement with cardiac system. For example, the first-in-class approved drug for MS, Fingolimod (FTY720), is known to be active against all S1P receptors except S1PR2[3,19]. Activation of S1PR3 by Fingolimod is associated with heart conditions such as bradycardia.[20,21] Hence, this limits the clinical use of Fingolimod. In contrast, second-generation S1P receptor modulators such as Siponimod, Ozanimod, and Ponesimod are more selective for S1PR1 and S1PR5 over S1PR2, S1PR3, and S1PR4, resulting in fewer side effects[9,11,12]. Understanding the mechanisms of action of these next-generation drugs is crucial for developing strategies to enhance drug selectivity in GPCR therapeutics.

Functional assays, such as the GTPγ[^{35}S]-binding assay, are commonly employed to assess the activity of ligands against GPCRs[22,23]. When agonists bind to GPCRs, they induce conformational changes in the receptor, leading to the dissociation of the α subunit from the β and γ subunits of the heterotrimeric G protein complex[24]. This assay measures the radioactivity of GTPγ[^{35}S] that binds to the Gα subunit by displacing GDP from the binding pocket. However, these assays cannot differentiate whether G-protein activation failed due to the ligand not binding to the active site or, failing to induce the necessary structural changes despite binding. Siponimod is a second-generation approved treatment in adults for the relapsing forms of Multiple Sclerosis (MS) that

includes the clinically isolated syndrome, relapsing- remitting MS, and active secondary progressive MS[25,26]. *In vitro* studies using GTPγ[^{35}S]-binding assay reported that the half maximal effective concentrations (EC50) for Siponimod in human S1PR1 and S1PR5 are ≈0.46 nM and ≈ 0.3 nM, respectively. In contrast, the EC50 for S1PR2, S1PR3 and S1PR4 are > 10,000 nM, > 1111 nM and ≈383.7 nM, respectively[22,27]. So, it is evident that Siponimod selectively modulates S1PR1 and S1PR5 over S1PR2, S1PR3, and S1PR4. Also, radioligand binding assays confirm Siponimod's binding at the active site (i.e., the S1P binding site) of human S1P1 and S1P5 but the results for the same are not available for the other three receptors that Siponimod fails to modulate[27]. Therefore, the precise mechanism behind Siponimod's selectivity remains unclear, highlighting the need for further investigation to understand its mode of action and improve drug design strategies in GPCR therapeutics.

Meticulously designed computational studies have the potential to complement experimental methods and help overcome their limitations, particularly in the context of drug design[28]. In this study, we utilized a range of bioinformatics and computational chemistry techniques to explore the potential binding of Siponimod to the active site of S1PR1 and S1PR2. Previous computational approaches suggested that Siponimod's lower selectivity for S1PR2 might be due to steric clashes with a phenylalanine residue (F274) upon docking to its active site[29]. However, this hypothesis was based on an engineered active site of S1PR2 derived from a cryo-EM structure of Siponimod-bound S1PR1. Recently, the cryo-EM structure of S1P-bound S1PR2 has been resolved[17], providing an opportunity to investigate Siponimod's binding potential to S1PR2 using more accurate computational methods. Our analyses, involving structure modeling, molecular docking, and microsecond timescale atomistic Molecular Dynamics (MD) simulations, indicate that Siponimod can indeed bind strongly to the active site of S1PR2. Despite this strong binding, our results show that Siponimod fails to induce the necessary conformational changes in the activation switches of S1PR2. We propose that Siponimod's inability to activate S1PR2 is due to its interaction with specific residues within the active site. These residues could be targeted in future drug design efforts to enhance selectivity.

II. METHODS AND TOOLS

Sequence alignment of S1PR1 and S1PR2 was performed using NCBI BLASTp[30,31] server to determine the percentage sequence similarity between the two S1P receptors.

Structure modelling of S1PR1 and S1PR2: The general architecture of the seven transmembrane helices along with extracellular and intracellular loops in S1PRs are illustrated in Figure 1a. Important transmission switches, ERY(H) and NPxxY motifs along with most conserved residues as per Ballesteros Weinstein (BW)[32] numbering schemes are depicted in the snake plot[33,34]. For *in silico* investigations, we selected the latest cryo-EM structures of human S1PR1 (PDB ID: 7TD3[29]) and S1PR2 (PDB ID: 7T6B[17]) that are complexed with the native ligand S1P and with the G proteins in the cytoplasmic regions. This will ensure that the S1P receptors are in their respective active state conformations. For the next steps we focused only on the S1PR chains, i.e. chain D in 7TD3 and chain E in 7T6B. Missing residues in both the chains, except the highly disordered N and C terminal residues, were modelled using Swiss modeler server[35]. The final modeled S1PR1 and S1PR2 chains have 304 and 279 residues, respectively. The first 21 residues in the N-terminal are missing in final modelled S1PR1 and the first 11 N-terminal residues are missing in the final modelled S1PR2. The residue numbering was adjusted accordingly. The structural similarity between the final modeled structures of S1PR1 and S1PR2 was assessed using Foldseek[36]. Foldseek performs structural alignment by utilizing a structural alphabet that emphasizes tertiary interactions rather than the protein backbone. This method generates a TM-score[37] to quantify structural similarity, ranging from 0 to 1. A higher TM-score indicates greater structural similarity between the two proteins.

Molecular docking: Molecular docking was performed using AutoDock VINA[38,39] utility in UCSF Chimera[40] with default settings. S1P and Siponimod were docked at the S1P binding site (illustrated in Figure 1c) of both S1PR1 and S1PR2. Different non-covalent interactions forming between the docked ligand and the binding site residues were analyzed using Protein-Ligand Interaction Profiler (PLIP)[41]. The docked poses with the highest docking scores were used for building the initial structures for performing MD simulations. To mimic the cellular environment in the MD simulations, ligand free and ligand bound receptors were embedded in lipid environment and surrounded by water as illustrated in Figure 1b. All-atom unbiased MD simulations were performed on six systems, viz., (i) Siponimod bound S1PR1 (Siponimod-S1PR1), (ii) Siponimod bound S1PR2 (Siponimod-S1PR2), (iii) S1P bound S1PR1 (S1P-S1PR1), (iv) S1P bound S1PR2 (S1P-S1PR2), (v) ligand free S1PR1 (apo S1PR1) and (vi) ligand free S1PR2 (apo S1PR2).

Setting up MD simulations: The MD systems were prepared using a set of utilities present in Ambertools22[42]. Force fields for S1P and Siponimod were generated with AM1-BCC charges[43,44] in antechamber[45,46]. Protein was embedded in the POPC (1-palmitoyl-2- oleoyl-sn-glycero-3-phosphocholine) layer with proper alignment using PACKMOL- Memgen[47] tool in Ambertools22. Lipid21 force field[48] was used for the lipid bilayer. The systems were hydrated with a three-point SPC/E[49,50] water model in a cubic box with 8 Å buffer. Chloride ions were added to neutralize the system. The AMBER readable topology and coordinate files of the systems were converted to GROMACS compatible format using ParmEd python utility. Minimization, NVT equilibration followed by NPT equilibration and NPT production run were carried out in GPU enabled GROMACS 2022.3[51–53] following well-established protocols as discussed in detail in the SI. For each of the six systems 1 μs long MD trajectory was generated for further analysis.

Analysing MD trajectories: The MD trajectories were visualized using Visual Molecular Dynamics (VMD 1.9.4) tool[54] and analyzed using GROMACS and Ambertools22.

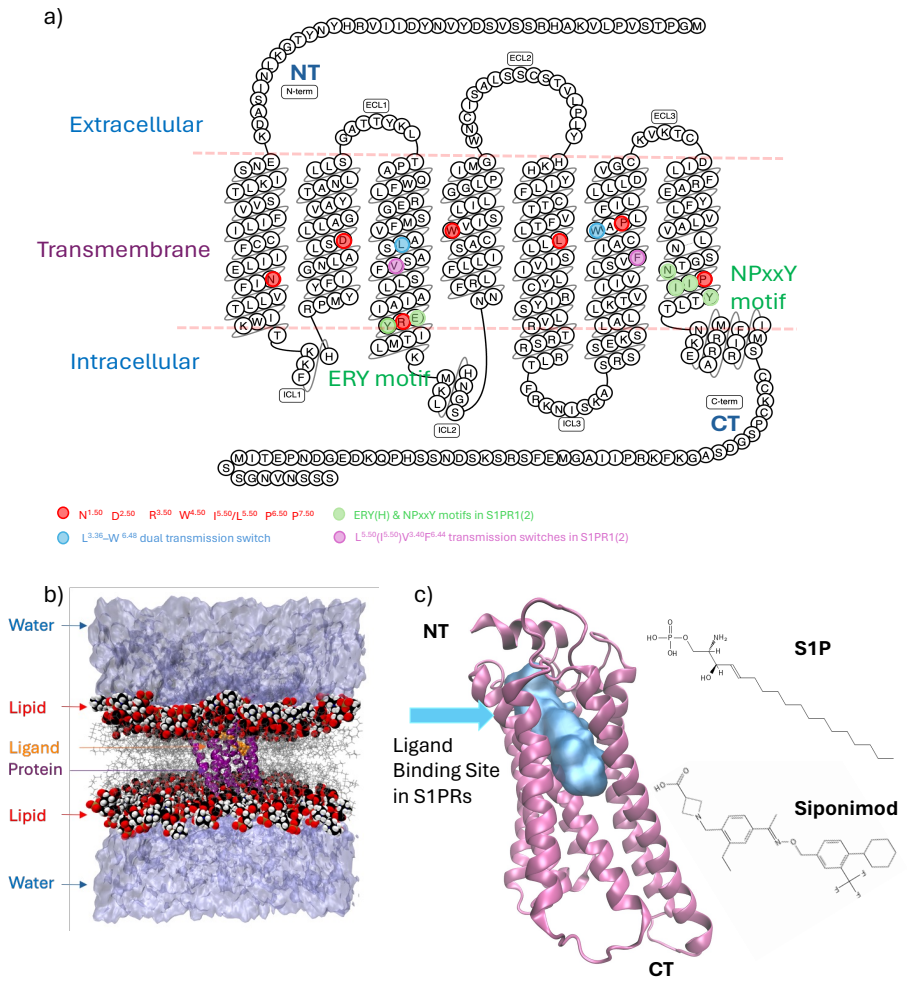

FIG. 1. System details for S1P receptors. a) Snake plot and a 3D representation depicting the most conserved residues of the Transmembrane (TM) helices in S1PRs (red), important toggle switches (blue) and conserved ERY(H) and NPxxY motifs (green) in S1PRs; b) MD simulation system consisting of ligand bound S1P receptors inside lipid in aqueous medium; c) S1P and Siponimod binds at the N-terminal (NT) end of the receptors occupying same binding pocket as shown in blue surface.

Fluctuations in receptors during the simulation trajectories were measured by Root Mean Square Displacement (RMSD) with respect to the initial structure and Root Mean Square Fluctuations (RMSF) averaged over the entire trajectory. For quantifying the relative dynamics of different parts of the receptors, Dynamic Cross- Correlation Maps (DCCM) and Principal Component Analysis (PCA)[55] were obtained using CPPTRAJ utility[56] from Ambertools22.

Relative binding free energies of the ligand-bound receptors were obtained from MMGBSA calculations[57] performed using the gmx_MMPBSA package[58]. A single trajectory approach using modified Gibbs-Boltzmann protocol was followed[59]. To understand the chemistry of ligand-protein interactions, the hydrogen bonds formed between the ligand and receptor residues were identified at every frame and persistent ones were shortlisted. Hydrogen bond length cut-off between the donor and acceptor atoms was set to 3.5 Å and the angle cutoff between donor-hydrogen-acceptor atoms was set to 30°.

III. RESULTS AND DISCUSSION

This study explores the selective modulation of S1PR1 over S1PR2 by Siponimod using a comprehensive array of *in silico* methods, including protein sequence and structure alignment, molecular docking, and all-atom conventional MD simulations. The BW numbering scheme is utilized in this article to identify the residues in the transmembrane helices.

A. Active sites of both S1PR1 and S1PR2 have high structural similarity

The sequence and structural similarities between the two S1P receptors, S1PR1 and S1PR2, were analyzed in detail. A sequence alignment using the NCBI BLASTp server reveals that these two sequences share only about 50% similarity (Figure SI 1). Despite this modest sequence similarity, the

proteins exhibit high structural similarity, as evidenced by a TM-score of 0.88 obtained from Foldseek (Figure SI 2). This is expected since both receptors are members of the S1P receptor sub-family. The transmembrane helices and the overall fold, particularly the configuration of the S1P binding pocket (the active site), are nearly identical in both receptors. Minor structural differences are primarily due to variations in the orientations of the extracellular (ECL) and intracellular (ICL) loops (Figure SI 2). Given the structural similarities of the active sites in S1PR1 and S1PR2 and considering that Siponimod binds to the active site of S1PR1, it is reasonable to hypothesize that Siponimod will also bind to the active site of S1PR2.

While most residues involved in ligand binding and activation mechanisms are conserved, the sequence alignment indicates a few notable differences (Figure SI 1). For example, leucine ($L^{7.39}$) in S1PR1 is replaced by phenylalanine ($F274/F^{7.39}$) in S1PR2, highlighted in pink in Figure SI 1. Other similar differences are discussed in the SI. Although both leucine and phenylalanine have hydrophobic side chains, phenylalanine's bulkier phenyl group was previously hypothesized[29] to cause a steric clash, preventing Siponimod from binding to the active site of S1PR2 based on studies using an engineered binding pocket. However, with the availability of the S1P-bound S1PR2 structure[17], we can now re-evaluate this hypothesis and determine whether Siponimod can indeed bind to the active site of S1PR2.

B. Molecular docking suggests Siponimod can bind strongly to the active sites of both S1PR1 and S1PR2

A recent study[27] reveals that the molecular docking analysis of diverse S1PR modulators to the active sites of both S1PR1 and S1PR5 exhibited a good correlation with experimental data. Therefore, we utilized molecular docking to compare the binding affinities of both S1P and Siponimod to the active sites of S1PR1 and S1PR2. At the outset of the discussion, it is important to note that experimentally determined structures of S1P-bound S1PR1 and S1PR2 were used in this study. The apo and Siponimod-bound systems for S1PR1 and S1PR2 were prepared from these S1P-bound protein structures, suggesting that the initial structures of S1PR1 and S1PR2 were already in an active conformation. Siponimod was then docked to the active conformations of both receptors. Both S1P and Siponimod occupy the same space inside the active site with polar head facing the extracellular region and the non-polar tails buried in the hydrophobic pocket near the transmission switches.

The binding affinity of Siponimod for S1PR2 (-13 kcal/mol) was ≈1.5 kcal/mol higher than that for S1PR1 (-11.7 kcal/mol). Additionally, contrary to the previous hypothesis[29], the docked pose of Siponimod showed no steric clashes with $F^{7.39}$ at the S1PR2 binding site (Figure 2c). These findings indicate that Siponimod not only binds to both receptors but also exhibits a slightly stronger binding affinity for S1PR2. A comparison of the ligand-protein interaction patterns of Siponimod with S1PR1 and S1PR2 shows that most of Siponimod's interactions with both the receptors are through pi-stacking and hydrophobic interactions, with additional salt bridge interactions with ARG^{ECL1} in S1PR2. This explains its higher binding affinity compared to S1PR1 (Figure 2a & Figure 2c). Of particular importance is Siponimod's hydrogen bond interaction with $ASN^{2.60}$ in both S1PR1 and S1PR2.

S1P engages the N-terminal residues by forming hydrogen bonds and salt bridges with its phosphate head group, and the hydrophobic residues of the receptors interact with the lipid-like tail of S1P (Figure 2b & Figure 2d). In S1PR2, a salt bridge between ARG^{NT} and the phosphate head of S1P is also observed.

To validate the docking protocol, the docked conformation of Siponimod in S1PR1 was compared with its conformation in the cryo-EM structure of Siponimod-bound S1PR1 (PDB ID 7TD4). Typically, an RMSD of less than 2 Å between the docked pose and the reference structure (i.e., ligand pose from the crystal structure) is considered sufficiently accurate for ligand docking[60,61]. For Siponimod, the hydrophobic tail of the docked pose aligned well with the crystal structure pose, though there was a noticeable shift in the hydrophilic head, resulting in an RMSD (symmetry corrected) of approximately 1.8 Å between the two poses (Figure SI 3), which is acceptable. Since the same docking protocol was used to obtain the Siponimod bound S1PR2 structure, its reliability is supported. However, a comparison of the interactions of docked Siponimod in S1PR1 with experimentally determined Siponimod bound S1PR1 interactions revealed that, due to a different orientation of the polar head group at the N-terminal in the docked structure, interactions with LYS^{NT}, ARG^{ECL1}, and GLY^{ECL1} were absent in the docked pose of Siponimod in S1PR1 (Figure 2e).

The degrees of freedom of the protein residues were not considered during the rigid docking process, resulting in a static depiction of protein-ligand interactions. To understand these interactions more precisely, it is essential to consider the dynamics of the protein upon ligand binding. Therefore, all-atom unbiased MD simulations of both ligand-free and ligand-bound (S1P & Siponimod) S1PR1 and S1PR2 proteins embedded within lipid bilayers were conducted. This approach enables the comparison of (a) the binding free energy of the ligands, (b) the persistence of various protein-ligand interactions, (c) the impact of ligand binding on the structural dynamics of protein residues, and (d) the coordinated motions of the transmembrane helices.

C. MD simulations confirm Siponimod's binding to the active site of S1PR2

The MD trajectories were examined for the extent of fluctuations. As expected, residues corresponding to the loop regions have higher freedom to move thus showing higher RMSF values in both S1PR1 and S1PR2 systems (Figure SI 4a & Figure SI 4b). In the case of S1PR1, the RMSD fluctuations stabilized after ≈200 ns in apo and S1P bound receptor and after ≈500 ns for the Siponimod bound receptor (Figure

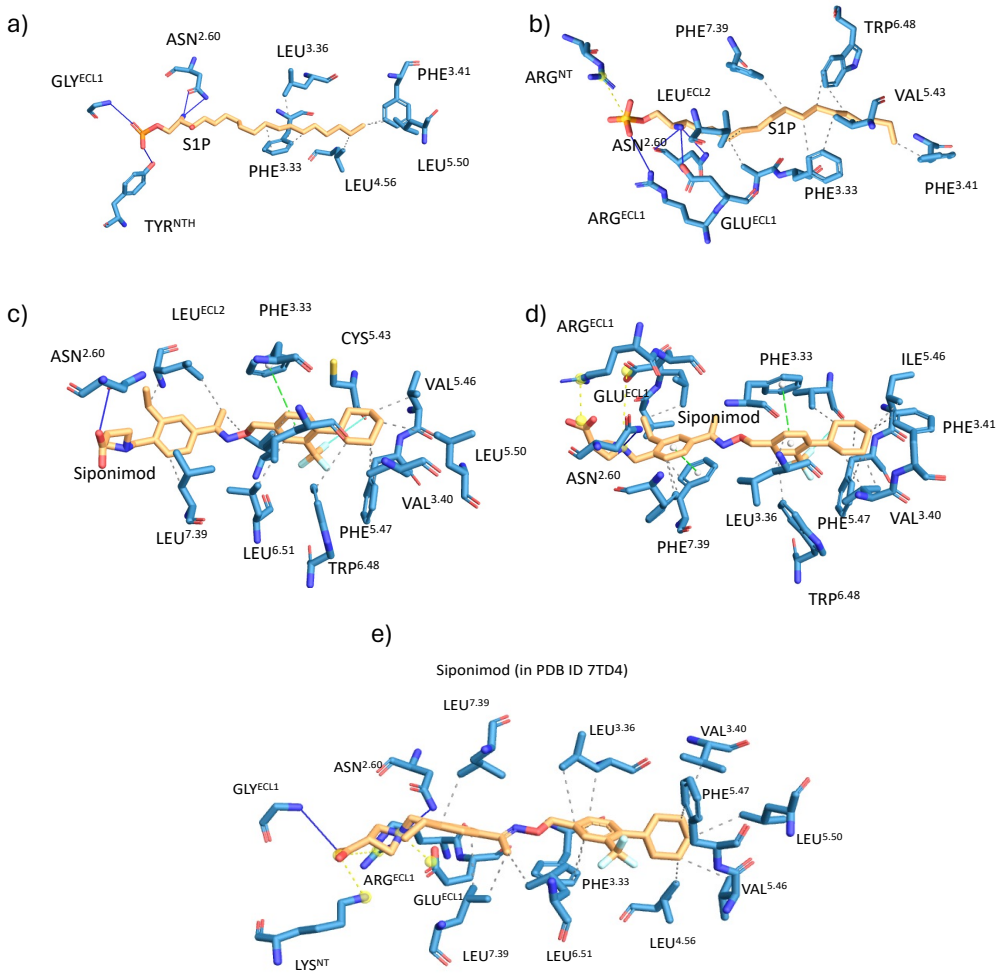

FIG. 2. PLIP analysis on the ligand bound S1PR1 and S1PR2 conformations obtained from docking: Hydrophilic head in S1P and Siponimod is engaged in hydrogen bonding with extracellular residues and the aliphatic chain is involved in hydrophobic interactions a) S1P bound S1PR1; b) S1P bound S1PR2; c) Siponimod bound S1PR1; d) Siponimod bound S1PR2; e) Siponimod bound S1PR1 in experimental structure.

SI 4c). RMSD fluctuations for all the three systems related to S1PR2 stabilized after ≈300 ns (Figure SI 4d). To maintain uniformity, MMGBSA calculations, along with pair-wise residue decomposition analysis (Figure 3), were performed on the last 500 ns (of the total 1 μs) trajectory, during which stable RMSD fluctuations were observed in all six cases (Figure 3). The relative binding free energies obtained from MMGBSA method ($\Delta G^{binding}_{MMGBSA}$) were also obtained for 5 short 20 ns replicas and are in good agreement with the values obtained from the 500 ns trajectory (Table SI 1). Siponimod binds strongly at the active sites of both the receptors S1PR1 ($\Delta G^{binding}_{MMGBSA} \approx$ -60.6 kcal/mol) and S1PR2 ($\Delta G^{binding}_{MMGBSA} \approx$ -67.8 kcal/mol) and its binding to S1PR2 is stronger than its binding to S1PR1. This correlates well with the binding affinities obtained from docking studies. As per the MMGBSA values, the native ligand S1P binds to both receptors with a stronger affinity compared to the approved drug Siponimod (Figure 3 and Table SI 1). Again, binding strength of S1P towards S1PR1 (-77.8 kcal/mol) is higher than that towards S1PR2 (-68.5 kcal/mol).

Our results also align well with the experimentally reported activity values, except for Siponimod-S1PR2 system. The pEC50 values for S1P and Siponimod against S1PR1 are 10.57 and 9.41, respectively (source: PHAROS database[62–64]). This indicates a higher affinity of S1P for S1PR1 compared to Siponimod. Additionally, the affinity of S1P for S1PR2 (pEC50 = 9.64) is reported to be[22,27] lower than its affinity for S1PR1. However, for Siponimod-S1PR2, the EC50 value is reported to be > 10000 nM. As previously mentioned, these values are derived from the GTPγ[^{35}S] functional assay, which does not necessarily evaluate whether Siponimod can bind to S1PR2, but only evaluates the activation of S1PR2 by Siponimod. Note that, evidence of S1P and Siponimod binding to the same active site in S1PR1 has been reported using competitive radioligand binding assays[22,27]. Cryo-EM structure of S1P-bound S1PR2 has also been solved[17]. But, to our knowledge, there is no reported study on Siponimod binding to S1PR2 using competitive radioligand binding assays or equivalent experimental methods.

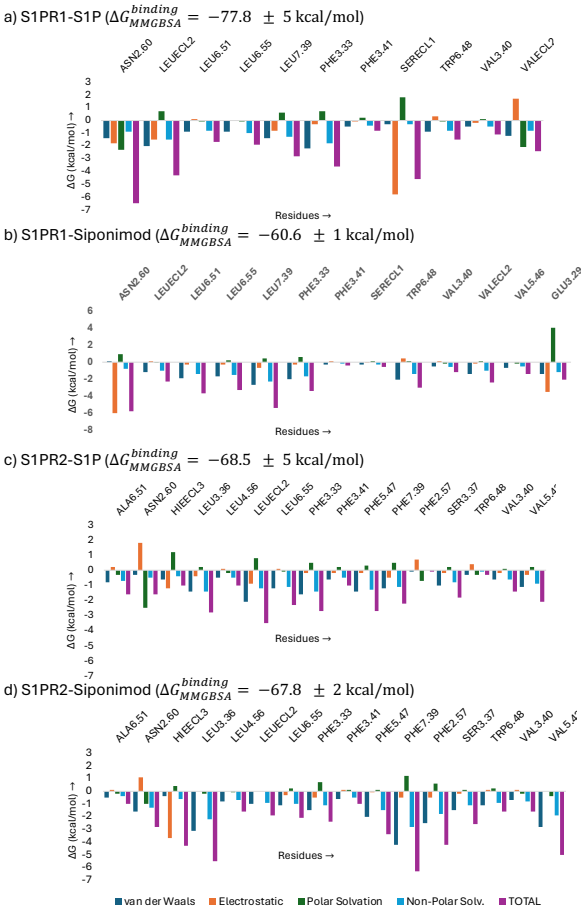

FIG. 3. Residue-wise decomposition of the ligand binding free energy obtained from MMGBSA method ($\Delta G^{binding}_{MMGBSA}$) performed on the last 500 ns of the 1 μs trajectory. For statistically meaningful results, five 20 ns replicas for each of the four ligand bound systems were run starting from well equilibrated structure. The relative binding free energies obtained from the replicas (Table SI 1) follows the same trend as reported here.

Hence, the experimental reports remain ambiguous regarding Siponimod's binding to S1PR2.

Computational studies performed in this work suggest that Siponimod can bind to the active site of S1PR2, while experimental reports indicate that Siponimod cannot modulate S1PR2 activity. To reconcile these findings, we aim to investigate whether Siponimod indeed binds to the active site of S1PR2 but fails to induce the structural changes necessary for modulation. The following sections will delve into these investigations, exploring the underlying mechanisms and potential implications.

D. Siponimod employs a different binding strategy than S1P at the active site of S1PR2

Pairwise energy decomposition values (Figure 3) suggest that Siponimod and S1P follow the same general strategy to bind to the active sites. In both the cases, the polar head part forms electrostatic interactions with the active site residues and the nonpolar tail part gets stabilized by hydrophobic interactions. The phosphate group on S1P ligand is involved in salt bridges and strong H-bonds interactions at the N- terminal of the receptors. In case of Siponimod also, the polar head is stabilized in the pocket through H-bond interactions.

TABLE I. Persistence of hydrogen bonds between the ligands (S1P or Siponimod) and important receptor residues viz. $ASN^{2.60}$ and HIS^{ECL3}. The numbers indicate the fraction of MD frames where the receptor residue is engaged in a hydrogen bonding interaction with the ligand bound at the active site.

	S1P-S1PR1	Siponimod-S1PR1	S1P-S1PR2	Siponimod-S1PR2
HIS^{ECL3}	NA	NA	0.1%	51%
$ASN^{2.60}$	55%	97%	45%	0.3%

Although the similar set of active site residues contribute towards binding of S1P and Siponimod, the chemical nature of interaction varies between the binding of S1P and Siponimod as evident in case of $ASN^{2.60}$ and HIS^{ECL3}. For instance, contribution of $ASN^{2.60}$ comes from polar solvation in S1P-S1PR2. On the contrary, it is mostly van der Waals and non-polar solvation in Siponimod-S1PR2 complex. This difference can be understood by the persistence of different hydrogen bonds (H-bond) that stabilize the ligand at the binding site. It is observed that a preserved H-bond between hydrophilic head of the ligands with $ASN^{2.60}$ is present in S1P-S1PR1, S1P- S1PR2 and Siponimod-S1PR1 systems, but not in Siponimod-S1PR2 system (occurrence < 1% in Table I).

The energy decomposition analysis (Figure 3) also suggests that HIS^{ECL3}(HIS271) has a large electrostatic contribution to Siponimod-S1PR2 interaction, but this contribution is less in case of S1P-S1PR2. Siponimod forms a hydrogen bond with HIS^{ECL3} in S1PR2 which is absent in case of S1P-S1PR2. It was observed during the trajectory analysis that HIS^{ECL3}, which was in proximity to S1P in S1PR2, flipped to a different orientation during the simulation and remained in that flipped state. However, this flip was not observed in Siponimod-bound S1PR2 due to the formation of an additional hydrogen bond between Siponimod's polar head and HIS^{ECL3}. Next, we evaluate how these subtle differences collectively limit Siponimod's ability to modulate S1PR2.

E. The binding of Siponimod and S1P differentially influences the structural dynamics of S1PR2

DCCM maps give an average picture of how each residue is moving with respect to each other during the trajectory. To understand the overall dynamics of residues across the cases, DCCM were generated for the initial 500 ns trajectory, during which most movements were observed to reach an equilibrated structure (Figure SI 5). In the ligand- free apo systems, the dynamics of ICL2 and ICL3, loops that interact with the Gα protein in the cytoplasm, remain uncorrelated with the dynamics of the rest of the receptor, except with the

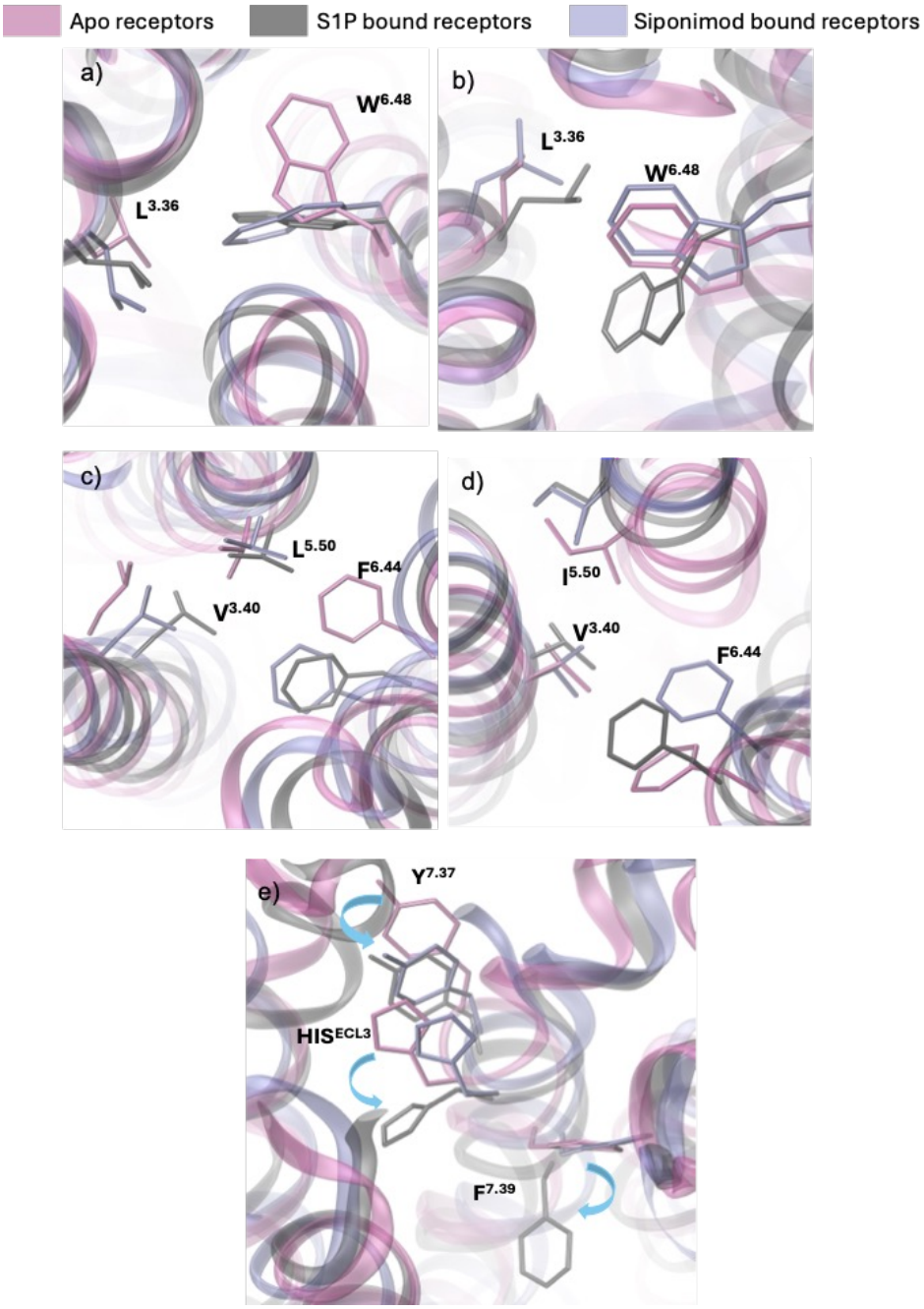

FIG. 4. Transmission switches in S1PR1 and S1PR2. a) $L^{3.36}$-$W^{6.48}$ switces exhibit similar flip in S1P and Siponimod bound S1PR1; b) $L^{3.36}$-$W^{6.48}$ switces exhibit different orientations in S1P and Siponimod bound S1PR2; c) S1P and Siponimod exhibiting similar structural changes in $L^{5.50}$-$V^{3.40}$-$F^{6.44}$ motif in S1PR1; d) S1P and Siponimod exhibiting slightly different structural changes in $I^{5.50}$-$V^{3.40}$-$F^{6.44}$ motif; e) HIS^{ECL3} flips in S1P bound S1PR2 leading to a conformation change in $Y^{7.37}$ and $F^{7.39}$. This movement is not observed in Siponimod bound S1PR2 case. Customized Collective Variables (CVs) were used to track the above switching events in the MD trajectories (see Figure SI 6).

NT residues (Figure SI 5a and SI 5d). This changes dramatically upon S1P binding. When S1P binds, the residues of ICL3 (and part of TM6) in S1PR1 (Figure SI 5b) and the residues of ICL2 in S1PR2 (Figure SI 5e) exhibit strongly anti-correlated movement with the rest of the receptor. Note that ICL3 is the longest cytoplasmic loop in S1PR1 while in S1PR2, both ICL2 and ICL3 are of similar length. Siponimod partially replicates this anti-correlated dynamic upon binding to S1PR1 (Figure SI 5c) but fails to produce a similar effect when Siponimod binds to S1PR2 (Figure SI 5f). Figure SI 5c illustrates that Siponimod binding to S1PR1 results in strong anti-correlated dynamics between the residues of ICL3 and

some residues of the active site distributed over ECL1, ECL2 and TM2. These results suggest that despite binding strongly at the active site, Siponimod fails to influence the dynamics of the G protein binding regions of S1PR2.

Activation of GPCRs, including the five S1P receptor family members, is known to take place through conformational changes of certain residues in the transmembrane helices. These residues are generally referred to as transmission switches[29,65–67]. Through MD simulations, we sought to determine the movements of these transmission switches across apo, S1P-bound and Siponimod-bound receptors, S1PR1 and S1PR2. The DCCM analyses indicate that, compared to S1P, Siponimod leads to a different conformation change in the transmission switches upon binding to S1PR2. The differential influence of S1P and Siponimod binding to the two key transmission switches in S1PRs known to differentiate the active vs inactive conformations are discussed below.

1. $W^{6.48}$ serves as a critical switch in GPCRs, including the S1P receptors, leading to receptor activation upon ligand binding[68,69]. Careful observations of the MD trajectories reveal that the $W^{6.48}$ switch is present in two distinctly different orientations when it is bound to S1P (active mode) vs. when ligand free (inactive mode). In S1PR1, the $W^{6.48}$ switch is found in its active mode when Siponimod is bound (Figure 4a). However, in S1PR2, the $W^{6.48}$ switch is not in its active mode when Siponimod is bound (Figure 4b). In addition, a conformational change in $L^{3.36}$ was noted as well (Figure 4a, 4b).

2. Another conserved motif, $P^{5.50}$-$I^{3.40}$-$F^{6.44}$, in GPCRs is known to play important role in receptor activation[70,71]. In case of S1PR1 and S1PR2, $L^{5.50}$-$V^{3.40}$-$F^{6.44}$ and $I^{5.50}$-$V^{3.40}$- $F^{6.44}$ motifs, respectively, play a similar role[72]. Similar to the $W^{6.48}$ switch, the $L^{5.50}$-$V^{3.40}$-$F^{6.44}$ switch in S1PR1 and the $I^{5.50}$-$V^{3.40}$-$F^{6.44}$ switch in S1PR2, are present in two distinctly different orientations when they are bound to S1P (active mode) vs. when ligand free (inactive mode). In S1PR1, the $L^{5.50}$-$V^{3.40}$-$F^{6.44}$ switch is found in its active mode (marked by changes in $F^{6.44}$ and $V^{3.40}$ orientations) when Siponimod is bound (Figure 4c). However, in S1PR2, the $I^{5.50}$-$V^{3.40}$-$F^{6.44}$ switch is not in its active mode (marked by a shift in $F^{6.44}$ orientations) when Siponimod is bound (Figure 4d).

Customized Collective Variables (CVs) were used to track the above switching events in the MD trajectories (Figure SI 6).

The relative movements of TM6 and TM7 in S1PRs are related to receptor activation[17,73]. We found that ligand binding induces conformational changes in $F^{6.44}$ and $V^{3.40}$, along with movements in $W^{6.48}$ and $L^{3.36}$, which determine the relative movements of TM6 and TM7.

Notably, in the Siponimod-S1PR2 system, TM6 exhibits an inward movement, reducing the distance to the TM7 helix, a behavior not observed in other ligand-bound systems (Figure SI 7). Given that the MD simulations were initiated from an active state conformation of the receptors, this implies that Siponimod binding at the active site of S1PR2 is not able to hold the active state conformation of S1PR2. Principal Component Analysis of the MD trajectories (Figure SI 8) suggests that in response to S1P binding at the active site, TM6 and TM7 move away from each other in opposite directions in both S1PR1 and S1PR2. Similar transmission switch dynamics are observed when Siponimod binds to S1PR1, but not when it binds to S1PR2.

In addition to the transmission switches, one notable movement in S1PR2 arises from HIS^{ECL3} (HIS271) which is present just before the start of TM7 helix. Note that, this is the same residue which is found to make stable hydrogen bond with Siponimod in S1PR2. In case of S1P bound S1PR2, the residue flipped to a different orientation resulting in a cascade of conformational changes in adjacent residues, $TYR^{7.37}$ and $PHE^{7.39}$, as shown in Figure 4e. However, a similar flip of HIS^{ECL3} is not observed in Siponimod bound S1PR2 or the apo state of the receptor. It seems that conformational changes in the HIS^{ECL3} and the associated residues ($TYR^{7.37}$ and $PHE^{7.39}$) are responsible for S1PR2 activation upon S1P binding. In an earlier study also, $PHE^{7.39}$ in S1PR2 was claimed to exhibit selectivity towards its inhibitor JTE-013. The study finds that the mutation F274I led to a decreased response to JTE-013 but an increased downstream activity upon FTY720-P binding[17]. Thus, it is reasonable to hypothesize that $PHE^{7.39}$ along with HIS^{ECL3} and $TYR^{7.37}$ can be leveraged to design selective modulators for S1P receptors. These residues can be used to optimize molecules to either enhance or reduce the binding to S1PR2, as required.

IV. CONCLUSION

Drug candidates can be optimized to address target selectivity on the grounds of shape of binding pockets, electrostatic properties on binding ligand, flexibility of residues inside pocket, hydration behavior of target protein, and allosteric inhibition[74]. Modifying the drug candidates to selectivity fit the target protein becomes increasingly intricate when dealing with targets and off-targets within same sub-family of proteins with significant amount of structural and sequence homology as observed in S1P receptors in this study. For large proteins such as GPCRs, although the scientific community is looking into allosteric modulators[75], discerning druggable metastable states or pinpointing effective allosteric pockets can be challenging.

Through this work we suggest utilizing computational methods like molecular docking and MD simulations to a) assess the binding strength of ligands inside protein pockets, b) understand the chemical nature of protein-ligand interactions and c) delineate the influence of ligand binding on the structural dynamics of the protein. In this study, we successfully demonstrated that, a strong ligand binding does not necessarily transfer to biological activity and MD simulations can shed more light on the induced structural changes required for target activity. In particular, we demonstrate that Siponimod binds strongly to the active site of S1PR2, but fails to trigger the conformational changes in the $W^{6.48}$ and the $I^{5.50}$-

$V^{3.40}$-$F^{6.44}$ transmission switches, which are essential for the rearrangement of the transmembrane helices TM6 and TM7 required to activate the receptor.

For further validating our hypothesis we propose performing radioligand competitive binding assays to confirm Siponimod's binding to S1PR2. Note that, similar assays have already been performed to check Siponimod's binding to other S1PRs (S1PR1 and S1PR5)[27]. Also enhanced MD simulations designed to study the ligand binding/unbinding kinetics can estimate the residence time of ligand in the protein pocket. Binding affinities, as obtained from conventional MD simulations performed in this work, when combined with the residence time details of the ligand can discern more accurate picture of protein-ligand interactions[76]. Such studies are beyond the scope of the present work. Nevertheless, with our current exercise we were able to leverage MD to compare the structural dynamics of the receptors, S1PR1 and S1PR2, when bound to S1P and Siponimod. We could infer that the structural dynamics of S1PR1 were similarly affected by both S1P and Siponimod binding, whereas S1PR2 responded differently to the binding of these two molecules. We could also observe that interaction of HIS^{ECL3} (HIS271) with Siponimod in S1PR2 was responsible for the difference in dynamics. We propose that three residues, $PHE^{7.39}$, HIS^{ECL3} and $TYR^{7.37}$, can be exploited to design selective modulators for S1P receptors.

SUPPORTING INFORMATION

See the "Supporting Information" material for Figure SI 1 - Figure SI 9, Table SI 1 and details of MD protocol used, sequence alignment of S1PR1 with respect to S1PR2 and the residues important for their activation mechanism, assessing System fluctuations via RMSD and RMSF analysis of MD trajectories, ligand binding free energies obtained from MMGBSA calculations, analyzing inter-residue dynamics using DCCM, and metastable states of ligand bound S1PR1 and S1PR2 using PCA analysis.

ACKNOWLEDGMENTS

We are grateful to Dr. Shubhandra Tripathi, Dr. Madhura Mohole, Dr. Srinath V. K. Kompella, Mr. Prasad Chodavarapu and Mr. Vikram Duvvoori for the invaluable discussions and constructive feedback during the preparation of manuscript.

DATA AVAILABILITY STATEMENT

PDB IDs for protein files used in the article are mentioned in main manuscript. MD simulation data can be made available on request.

AUTHOR DECLARATIONS

Conflict of Interest

All the authors are the employees of Aganitha, the company that holds interests in any commercial gains arising out of this work.

Author contributions

Kumari Soniya: Formal analysis (lead); Investigation (lead); Writing - original draft (lead); Writing – review & editing (equal). **Chanukya Nanduru**: Supervision (lead); Writing – review & editing (equal). **Antarip Halder**: Conceptualization (lead); Formal analysis (supporting); Writing – review & editing (equal).

[1] S. Saikia, M. Bordoloi, and R. Sarmah, "Established and in-trial GPCR families in clinical trials: A review for target selection," *Curr. Drug Targets* **20** (2018), 10.2174/1389450120666181105152439.

[2] K. Sriram and P. A. Insel, "G protein-coupled receptors as targets for approved drugs: How many targets and how many drugs?" *Mol. Pharmacol.* **93** (2018), 10.1124/mol.117.111062.

[3] A. S. Hauser, M. M. Attwood, M. Rask-Andersen, H. B. Schiöth, and D. E. Gloriam, "Trends in gpcr drug discovery: New agents, targets and indications," *Nat. Rev. Drug Discov.* **16** (2017), 10.1038/nrd.2017.178.

[4] T. Laeremans, Z. A. Sands, P. Claes, A. D. Blieck, S. D. Cesco, S. Triest, A. Busch, D. Felix, A. Kumar, V. P. Jaakola, and C. Menet, "Accelerating GPCR drug discovery with conformation-stabilizing VHHs," *Front. Mol. Biosci.* **9** (2022), 10.3389/fmolb.2022.863099.

[5] D. Yang, Q. Zhou, V. Labroska, S. Qin, S. Darbalaei, Y. Wu, E. Yuliantie, L. Xie, H. Tao, J. Cheng, Q. Liu, S. Zhao, W. Shui, Y. Jiang, and M. W. Wang, "G protein-coupled receptors: structure- and function-based drug discovery," *Signal. Transduct. Target. Ther.* **6** (2021), 10.1038/s41392-020-00435-w.

[6] K. Mendelson, T. Evans, and T. Hla, "Sphingosine 1-phosphate signalling," *Dev. (Camb.)* **141** (2014), 10.1242/dev.094805.

[7] J. G. Cyster and S. R. Schwab, "Sphingosine-1-phosphate and lymphocyte egress from lymphoid organs," *Annu. Rev. Immunol.* **30** (2012), 10.1146/annurev-immunol-020711-075011.

[8] R. Pappu, S. R. Schwab, I. Cornelissen, J. P. Pereira, J. B. Regard, Y. Xu, E. Camerer, Y. W. Zheng, Y. Huang, J. G. Cyster, and S. R. Coughlin, "Promotion of lymphocyte egress into blood and lymph by distinct sources of sphingosine-1-phosphate," *Science* **316** (2007), 10.1126/science.1139221.

[9] G. Álvarez Bravo, R. R. Cedeño, M. P. Casadevall, and L. Ramió-Torrentà, "Sphingosine-1-phosphate (S1P) and S1P signaling pathway modulators, from current insights to future perspectives," *Cells* **11** (2022), 10.3390/cells11132058.

[10] R. Roy, A. A. Alotaibi, and M. S. Freedman, "Sphingosine 1-phosphate receptor modulators for multiple sclerosis," *CNS Drugs* **35** (2021), 10.1007/s40263-021-00798-w.

[11] O. J. Kandjani, S. Yaqoubi, S. S. Vahdati, B. Borhannejad, S. Dastmalchi, and A. A. Alizadeh, "S1PR1 modulators in multiple sclerosis: Efficacy, safety, comparison, and chemical structure insights," *Eur. J. Med. Chem.* **250** (2023), 10.1016/j.ejmech.2023.115182.

[12] P. K. Coyle, M. S. Freedman, B. A. Cohen, B. A. Cree, and C. E. Markowitz, "Sphingosine 1-phosphate receptor modulators in multiple sclerosis treatment: A practical review," *Ann. Clin. Transl. Neurol.* **11** (2024), 10.1002/acn3.52017.

[13] Y. Liu, Y. Zhi, H. Song, M. Zong, J. Yi, G. Mao, L. Chen, and G. Huang, "S1PR1 promotes proliferation and inhibits apoptosis of esophageal squamous cell carcinoma through activating STAT3 pathway," *J. Exp. Clin. Cancer Res.* **38** (2019), 10.1186/s13046-019-1369-7.

[14] M. Hao, R. Fu, J. Tai, Z. Tian, X. Yuan, Y. Chen, M. Wang, H. Jiang, M. Ji, F. Lai, N. Xue, L. Bai, Y. Zhu, X. Lv, X. Chen, and J. Jin, "S1PR1

serves as a viable drug target against pulmonary fibrosis by increasing the integrity of the endothelial barrier of the lung," *Acta Pharm. Sin. B.* **13** (2023), 10.1016/j.apsb.2022.10.006.

[15]V. Constantinescu, R. Haase, K. Akgün, and T. Ziemssen, "S1p receptor modulators and the cardiovascular autonomic nervous system in multiple sclerosis: a narrative review," *Ther. Adv. Neurol. Disord.* **15** (2022), 10.1177/17562864221133163.

[16]D. Mazurais, P. Robert, B. Gout, I. Berrebi-Bertrand, M. P. Laville, and T. Calmels, "Cell type-specific localization of human cardiac s1p receptors," *J. Histochem. Cytochem.* **50** (2002), 10.1177/002215540205000507.

[17]H. Chen, K. Chen, W. Huang, L. M. Staudt, J. G. Cyster, and X. Li, "Structure of s1pr2–heterotrimeric g13 signaling complex," *Sci. Adv.* **8** (2022), 10.1126/sciadv.abn0067.

[18]M. Pang, C. Li, D. Zheng, Y. Wang, J. Wang, W. Zhang, F. Li, and H. Jing, "S1PR2 knockdown promotes migration and invasion in multiple myeloma cells via NF-κB activation," *Cancer Manag. Res.* **12** (2020), 10.2147/CMAR.S237330.

[19]S. Mandala, R. Hajdu, J. Bergstrom, E. Quackenbush, J. Xie, J. Milligan, R. Thornton, G. J. Shei, D. Card, C. A. Keohane, M. Rosenbach, J. Hale, C. L. Lynch, K. Rupprecht, W. Parsons, and H. Rosen, "Alteration of lymphocyte trafficking by sphingosine-1-phosphate receptor agonists," *Science* **296** (2002), 10.1126/science.1070238.

[20]J. Chun and H. P. Hartung, "Mechanism of action of oral fingolimod (FTY720) in multiple sclerosis," *Clin. Neuropharmacol.* **33** (2010), 10.1097/WNF.0b013e3181cbf825.

[21]L. Kappos, J. Antel, G. Comi, X. Montalban, P. O'Connor, C. H. Polman, T. Haas, A. A. Korn, G. Karlsson, and E. W. Radue, "Oral fingolimod (FTY720) for relapsing multiple sclerosis," *N. Engl. J. Med.* **355** (2006), 10.1056/nejmoa052643.

[22]P. Gergely, B. Nuesslein-Hildesheim, D. Guerini, V. Brinkmann, M. Traebert, C. Bruns, S. Pan, N. S. Gray, K. Hinterding, N. G. Cooke, A. Groenewegen, A. Vitaliti, T. Sing, O. Luttringer, J. Yang, A. Gardin, N. Wang, W. J. Crumb, M. Saltzman, M. Rosenberg, and E. Wallström, "The selective sphingosine 1-phosphate receptor modulator BAF312 redirects lymphocyte distribution and has species-specific effects on heart rate," *Br. J. Pharmacol.* **167** (2012), 10.1111/j.1476-5381.2012.02061.x.

[23]C. Harrison and J. R. Traynor, "The [^{35}S]GTPγS binding assay: Approaches and applications in pharmacology," *Life Sci.* **74** (2003), 10.1016/j.lfs.2003.07.005.

[24]D. Hilger, M. Masureel, and B. K. Kobilka, "Structure and dynamics of GPCR signaling complexes," *Nat. Struct. Mol. Biol.* **25** (2018), 10.1038/s41594-017-0011-7.

[25]L. Kappos, A. Bar-Or, B. A. Cree, R. J. Fox, G. Giovannoni, R. Gold, P. Vermersch, D. L. Arnold, S. Arnould, T. Scherz, C. Wolf, E. Wallström, F. Dahlke, A. Achiron, L. Achtnichts, K. Agan, G. Akman-Demir, A. B. Allen, J. P. Antel, A. R. Antiguedad, M. Apperson, A. M. Applebee, G. I. Ayuso, M. Baba, O. Bajenaru, R. Balasa, B. P. Balci, M. Barnett, A. Bass, V. U. Becker, M. Bejinariu, F. T. Bergh, A. Bergmann, E. Bernitsas, A. Berthele, V. Bhan, F. Bischof, R. J. Bjork, G. Blevins, M. Boehringer, T. Boerner, R. Bonek, J. D. Bowen, A. Bowling, A. N. Boyko, C. Boz, V. Bracknies, S. Braune, V. B. Morra, B. Brochet, W. Brola, P. K. Brownstone, M. Brozman, D. Brunet, I. Buraga, M. Burnett, M. Buttmann, H. Butzkueven, J. Cahill, J. C. Calkwood, W. Camu, M. Cascione, G. Castelnovo, D. Centonze, J. Cerqueira, A. Chan, A. Cimprichova, S. Cohan, G. Comi, J. Conway, J. A. Cooper, J. Corboy, J. Correale, B. Costell, D. A. Cottrell, P. K. Coyle, M. Craner, L. Cui, L. Cunha, A. Czlonkowska, A. M. da Silva, J. de Sa, J. de Seze, M. Debouverie, J. Debruyne, D. Decoo, G. Defer, T. Derfuss, N. H. Deri, B. Dihenia, P. Dioszeghy, V. Donath, B. Dubois, M. Duddy, P. Duquette, G. Edan, H. Efendi, S. Elias, P. J. Emrich, B. C. Estruch, E. P. Evdoshenko, J. Faiss, A. S. Fedyanin, W. Feneberg, J. Fermont, O. F. Fernandez, F. C. Ferrer, K. Fink, H. Ford, C. Ford, A. Francia, M. Freedman, B. Frishberg, S. Galgani, G. P. Garmany, K. Gehring, J. Gitt, C. Gobbi, L. P. Goldstick, R. A. Gonzalez, F. Grandmaison, N. Grigoriadis, O. Grigorova, L. M. E. Grimaldi, J. Gross, K. Gross-Paju, M. Gudesblatt, D. Guillaume, J. Haas, V. Hancinova, A. Hancu, O. Hardiman, A. Harmjanz, F. R. Heidenreich, G. J. Hengstman, J. Herbert, M. Herring, S. Hodgkinson, O. M. Hoffmann, W. E. Hofmann, W. D. Honeycutt, L. H. Hua, D. Huang, Y. Huang, D. R. Huang, R. Hupperts, P. Imre, A. K. Jacobs, G. Jakab, E. Jasinska, K. Kaida, J. Kalnina, A. Kaprelyan, G. Karelis, D. Karussis, A. Katz, F. A. Khabirov, B. Khatri, T. Kimura, I. Kister, R. Kizlaitiene, E. Klimova, J. Koehler, A. Komatineni, A. Kornhuber, K. Kovacs, A. Koves, W. Kozubski, G. Krastev, L. B. Krupp, E. Kurca, C. Lassek, G. Laureys, L. Lee, E. Lensch, F. Leutmezer, H. Li, R. A. Linker, M. Linnebank, P. Liskova, C. Llanera, J. Lu, A. Lutterotti, J. Lycke, R. Macdonell, M. Maciejowski, M. Maeurer, R. V. Magzhanov, E. M. Maida, L. Malciene, Y. Mao-Draayer, G. A. Marfia, C. Markowitz, V. Mastorodimos, K. Matyas, J. Meca-Lallana, J. A. G. Merino, I. G. Mihetiu, I. Milanov, A. E. Miller, A. Millers, M. Mirabella, M. Mizuno, X. Montalban, L. Montoya, M. Mori, S. Mueller, J. Nakahara, Y. Nakatsuji, S. Newsome, R. Nicholas, A. S. Nielsen, E. Nikfekr, U. Nocentini, C. Nohara, K. Nomura, M. M. Odinak, T. Olsson, B. W. van Oosten, C. Oreja-Guevara, P. Oschmann, J. Overell, A. Pachner, G. Panczel, M. Pandolfo, C. Papeix, L. Patrucco, J. Pelletier, R. Piedrabuena, M. Pless, U. Polzer, K. Pozsegovits, D. Rastenyte, S. Rauer, G. Reifschneider, R. Rey, S. A. Rizvi, D. Robertson, J. M. Rodriguez, D. Rog, H. Roshanisefat, V. Rowe, C. Rozsa, S. Rubin, S. Rusek, F. Saccà, T. Saida, A. V. Salgado, V. E. F. Sanchez, K. Sanders, M. Satori, D. V. Sazonov, E. A. Scarpini, E. Schlegel, M. Schluep, S. Schmidt, E. Scholz, H. M. Schrijver, M. Schwab, R. Schwartz, J. Scott, K. Selmaj, S. Shafer, B. Sharrack, I. A. Shchukin, Y. Shimizu, P. Shotekov, A. Siever, K. O. Sigel, S. Silliman, M. Simo, M. Simu, V. Sinay, A. E. Siquier, A. Siva, O. Skoda, A. Solomon, M. Stangel, D. Stefoski, B. Steingo, I. D. Stolyarov, P. Stourac, K. Strassburger-Krogias, E. Strauss, O. Stuve, I. Tarnev, A. Tavernarakis, C. R. Tello, M. Terzi, V. Ticha, M. Ticmeanu, K. Tiel-Wilck, T. Toomsoo, N. Tubridy, M. J. Tullman, H. Tumani, P. Turcani, B. Turner, A. Uccelli, F. J. O. Urtaza, M. Vachova, A. Valikovics, S. Walter, B. V. Wijmeersch, L. Vanopdenbosch, J. R. Weber, S. Weiss, R. Weissert, P. Vermersch, T. West, H. Wiendl, S. Wiertlewski, B. Wildemann, B. Willekens, L. H. Visser, G. Vorobeychik, X. Xu, T. Yamamura, Y. N. Yang, S. M. Yelamos, M. Yeung, A. Zacharias, M. Zelkowitz, U. Zettl, M. Zhang, H. Zhou, U. Zieman, and T. Ziemssen, "Siponimod versus placebo in secondary progressive multiple sclerosis (EXPAND): a double-blind, randomised, phase 3 study," *The Lancet.* **391** (2018), 10.1016/S0140-6736(18)30475-6.

[26]E. R. Hammond, "Perspectives on safety and efficacy-the BOLD phase 2 extension study of siponimod in relapsing-remitting multiple sclerosis," *JAMA Neurol.* **73** (2016), 10.1001/jamaneurol.2016.2284.

[27]J. V. Selkirk, A. Bortolato, Y. G. Yan, N. Ching, and R. Hargreaves, "Competitive binding of ozanimod and other sphingosine 1-phosphate receptor modulators at receptor subtypes 1 and 5," *Front. Pharmacol.* **13** (2022), 10.3389/fphar.2022.892097.

[28]V. T. Sabe, T. Ntombela, L. A. Jhamba, G. E. Maguire, T. Govender, T. Naicker, and H. G. Kruger, "Current trends in computer aided drug design and a highlight of drugs discovered via computational techniques: A review," *Eur. J. Med. Chem.* **224** (2021), 10.1016/j.ejmech.2021.113705.

[29]S. Liu, N. Paknejad, L. Zhu, Y. Kihara, M. Ray, J. Chun, W. Liu, R. K. Hite, and X. Y. Huang, "Differential activation mechanisms of lipid GPCRs by lysophosphatidic acid and sphingosine 1-phosphate," *Nat. Commun.* **13** (2022), 10.1038/s41467-022-28417-2.

[30]A. Jacob, J. Lancaster, J. Buhler, B. Harris, and R. D. Chamberlain, "Mercury BLASTP: Accelerating protein sequence alignment," *ACM Trans. Reconfigurable Technol. Syst.* **1** (2008), 10.1145/1371579.1371581.

[31]A. Mahram and M. C. Herbordt, "NCBI BLASTP on high-performance reconfigurable computing systems," *ACM Trans. Reconfigurable Technol. Syst.* **7** (2015), 10.1145/2629691.

[32]J. A. Ballesteros and H. Weinstein, "[19] integrated methods for the construction of three-dimensional models and computational probing of structure-function relations in g protein-coupled receptors," (Academic Press, 1995) pp. 366–428.

[33]F. Horn, J. Weare, M. W. Beukers, S. Hörsch, A. Bairoch, W. Chen, Edvardsen, F. Campagne, and G. Vriend, "GPCRDB: An information system for g protein-coupled receptors," *Nucleic Acids Res.* **26** (1998), 10.1093/nar/26.1.275.

[34]G. Pándy-Szekeres, J. Caroli, A. Mamyrbekov, A. A. Kermani, G. M. Keseru, A. J. Kooistra, and D. E. Gloriam, "GPCRdb in 2023: state-specific structure models using AlphaFold2 and new ligand resources," *Nucleic Acids Res.* **51** (2023), 10.1093/nar/gkac1013.

[35]A. Waterhouse, M. Bertoni, S. Bienert, G. Studer, G. Tauriello, R. Gumienny, F. T. Heer, T. A. D. Beer, C. Rempfer, L. Bordoli, R. Lepore, and T. Schwede, "SWISS-MODEL: Homology modelling of protein structures and complexes," *Nucleic Acids Res.* **46** (2018), 10.1093/nar/gky427.

[36]M. van Kempen, S. S. Kim, C. Tumescheit, M. Mirdita, J. Lee, C. L. Gilchrist, J. Söding, and M. Steinegger, "Fast and accurate protein structure search with foldseek," *Nat. Biotechnol.* **42** (2024), 10.1038/s41587-023-01773-0.

[37]Y. Zhang and J. Skolnick, "Scoring function for automated assessment of protein structure template quality," *Proteins: Struct. Funct. Genet.* **57** (2004), 10.1002/prot.20264.

[38]J. Eberhardt, D. Santos-Martins, A. F. Tillack, and S. Forli, "AutoDock Vina 1.2.0: new docking methods, expanded force field, and python bindings," *J. Chem. Inf. Model.* **61** (2021), 10.1021/acs.jcim.1c00203.

[39]S. Tang, R. Chen, M. Lin, Q. Lin, Y. Zhu, J. Ding, H. Hu, M. Ling, and J. Wu, "Accelerating AutoDock vina with GPUs," *Molecules* **27** (2022), 10.3390/molecules27093041.

[40]E. F. Pettersen, T. D. Goddard, C. C. Huang, G. S. Couch, D. M. Greenblatt, E. C. Meng, and T. E. Ferrin, "UCSF Chimera - a visualization system for exploratory research and analysis," *J. Comput. Chem.* **25** (2004), 10.1002/jcc.20084.

[41]S. Salentin, S. Schreiber, V. J. Haupt, M. F. Adasme, and M. Schroeder, "PLIP: Fully automated protein-ligand interaction profiler," *Nucleic Acids Res.* **43** (2015), 10.1093/nar/gkv315.

[42]D. A. Case, H. M. Aktulga, K. Belfon, I. Y. Ben-Shalom, J. T. Berryman, S. R. Brozell, D. S. Cerutti, T. E. C. III, G. A. Cisneros, V. W. D. Cruzeiro, T. A. Darden, N. Forouzesh, G. Giambaşu, T. Giese, M. K. Gilson, H. Gohlke, A. W. Goetz, J. Harris, S. Izadi, S. A. Izmailov, K. Kasavajhala, M. C. Kaymak, E. King, A. Kovalenko, T. Kurtzman, T. S. Lee, P. Li, C. Lin, J. Liu, T. Luchko, R. Luo, M. Machado, V. Man, M. Manathunga, K. M. Merz, Y. Miao, O. Mikhailovskii, G. Monard, H. Nguyen, K. A. O'Hearn, A. Onufriev, F. Pan, S. Pantano, R. Qi, A. Rahnamoun, D. R. Roe, A. Roitberg, C. Sagui, S. Schott-Verdugo, A. Shajan, J. Shen, C. L. Simmerling, N. R. Skrynnikov, J. Smith, J. Swails, R. C. Walker, J. Wang, J. Wang, H. Wei, X. Wu, Y. Wu, Y. Xiong, Y. Xue, D. M. York, S. Zhao, Q. Zhu, and P. A. Kollman, *Amber 2022* (2022).

[43]A. Jakalian, B. L. Bush, D. B. Jack, and C. I. Bayly, "Fast, efficient generation of high-quality atomic charges. AM1-BCC Model: I. method," *J. Comput. Chem.* **21** (2000), 10.1002/(SICI)1096-987X(20000130)21:2<132::AID-JCC5>3.0.CO;2-P.

[44]A. Jakalian, D. B. Jack, and C. I. Bayly, "Fast, efficient generation of high-quality atomic charges. aM1-BCC model: II. parameterization and validation," *J. Comput. Chem.* **23** (2002), 10.1002/jcc.10128.

[45]J. Wang, R. M. Wolf, J. W. Caldwell, P. A. Kollman, and D. A. Case, "Development and testing of a general amber force field," *J. Comput. Chem.* **25** (2004), 10.1002/jcc.20035.

[46]J. Wang, W. Wang, P. A. Kollman, and D. A. Case, "Automatic atom type and bond type perception in molecular mechanical calculations," *J. Mol. Graph. Model.* **25** (2006), 10.1016/j.jmgm.2005.12.005.

[47]S. Schott-Verdugo and H. Gohlke, "PACKMOL-Memgen: A simple-to-use, generalized workflow for membrane-protein-lipid-bilayer system building," *J. Chem. Inf. Model.* **59** (2019), 10.1021/acs.jcim.9b00269.

[48]C. J. Dickson, R. C. Walker, and I. R. Gould, "Lipid21: Complex lipid membrane simulations with AMBER," *J. Chem. Theory Comput.* **18** (2022), 10.1021/acs.jctc.1c01217.

[49]H. J. Berendsen, J. R. Grigera, and T. P. Straatsma, "The missing term in effective pair potentials," *J. Phys. Chem.* **91** (1987), 10.1021/j100308a038.

[50]K. Takemura and A. Kitao, "Effects of water model and simulation box size on protein diffusions motions," *J. Phys. Chem. B.* **111** (2007), 10.1021/jp0756247.

[51]P. Bauer, B. Hess, and E. Lindahl, "GROMACS 2022.3 source code," (2022).

[52]H. J. Berendsen, D. van der Spoel, and R. van Drunen, "GROMACS: A message-passing parallel molecular dynamics implementation," *Comput. Phys. Commun.* **91** (1995), 10.1016/0010-4655(95)00042-E.

[53]H. Bekker, H. Berendsen, E. Dijkstra, S. Achterop, R. v. Vondrumen, D. Vanderspoel, A. Sijbers, H. Keegstra, and M. Renardus, English"GROMACS - a paralel computer for molecular-dynamics simulations," in English*PHYSICS COMPUTING '92*, edited by R. DeGroot and J. Nadrchal (World Scientific Publishing, 1993) pp. 252–256, 4th International Conference on Computational Physics (PC 92) ; Conference date: 24-08-1992 Through 28-08-1992.

[54]W. Humphrey, A. Dalke, and K. Schulten, "VMD: Visual molecular dynamics," *J. Mol. Graph.* **14** (1996), 10.1016/0263-7855(96)00018-5.

[55]K. Pearson, "LIII. on lines and planes of closest fit to systems of points in space," *Lond. Edinb. Dubl. Phil. Mag* **2** (1901), 10.1080/14786440109462720.

[56]D. R. Roe and T. E. Cheatham, "PTRAJ and CPPTRAJ: Software for processing and analysis of molecular dynamics trajectory data," *J. Chem. Theory Comput.* **9** (2013), 10.1021/ct400341p.

[57]B. R. Miller, T. D. McGee, J. M. Swails, N. Homeyer, H. Gohlke, and A. E. Roitberg, "MMPBSA.py: An efficient program for end-state free energy calculations," *J. Chem. Theory Comput.* **8**, 3314–3321 (2012).

[58]M. S. Valdés-Tresanco, M. E. Valdés-Tresanco, P. A. Valiente, and E. Moreno, "Gmx$_{MMPBSA}$: A new tool to perform end-state free energy calculations with GROMACS," *J. Chem. Theory Comput.* **17** (2021), 10.1021/acs.jctc.1c00645.

[59]A. Onufriev, D. Bashford, and D. A. Case, "Exploring protein native states and large-scale conformational changes with a modified generalized born model," *Proteins: Struct., Funct., Bioinf.* **55** (2004), 10.1002/prot.20033.

[60]G. Corso, H. Stärk, B. Jing, R. Barzilay, and T. Jaakkola, "Diffdock: Diffusion steps, twists, and turns for molecular docking," (2023), arXiv:2210.01776 [q-bio.BM].

[61]H. Cai, C. Shen, T. Jian, X. Zhang, T. Chen, X. Han, Z. Yang, W. Dang, C.-Y. Hsieh, Y. Kang, P. Pan, X. Ji, J. Song, T. Hou, and Y. Deng, "Carsidock: a deep learning paradigm for accurate protein–ligand docking and screening based on large-scale pre-training," *Chem. Sci.* **15**, 1449–1471 (2024).

[62]T. K. Sheils, S. L. Mathias, K. J. Kelleher, V. B. Siramshetty, D. T. Nguyen, C. G. Bologa, L. J. Jensen, D. Vidović, A. Koleti, S. C. Schürer, A. Waller, J. J. Yang, J. Holmes, G. Bocci, N. Southall, P. Dharkar, E. Mathé, A. Simeonov, and T. I. Oprea, "TCRD and pharos 2021: Mining the human proteome for disease biology," *Nucleic Acids Res.* **49** (2021), 10.1093/nar/gkaa993.

[63]D. T. Nguyen, S. Mathias, C. Bologa, S. Brunak, N. Fernandez, A. Gaulton, A. Hersey, J. Holmes, L. J. Jensen, A. Karlsson, G. Liu, A. Ma'ayan, G. Mandava, S. Mani, S. Mehta, J. Overington, J. Patel, A. D. Rouillard, S. Schürer, T. Sheils, A. Simeonov, L. A. Sklar, N. Southall, O. Ursu, D. Vidovic, A. Waller, J. Yang, A. Jadhav, T. I. Oprea, and R. Guha, "Pharos: Collating protein information to shed light on the druggable genome," *Nucleic Acids Res.* **45** (2017), 10.1093/nar/gkw1072.

[64]K. J. Kelleher, T. K. Sheils, S. L. Mathias, J. J. Yang, V. T. Metzger, V. B. Siramshetty, D. T. Nguyen, L. J. Jensen, D. Vidović, S. C. Schürer, J. Holmes, K. R. Sharma, A. Pillai, C. G. Bologa, J. S. Edwards, E. A. Mathe, and T. I. Oprea, "Pharos 2023: an integrated resource for the understudied human proteome," *Nucleic Acids Res.* **51** (2023), 10.1093/nar/gkac1033.

[65]B. Wingert, P. Doruker, and I. Bahar, "Activation and speciation mechanisms in class A GPCRs," *J. Mol. Biol.* **434** (2022), 10.1016/j.jmb.2022.167690.

[66]X. Deupi and J. Standfuss, "Structural insights into agonist-induced activation of g-protein-coupled receptors," *Curr. Opin. Struct. Biol.* **21** (2011), 10.1016/j.sbi.2011.06.002.

[67]A. Mitra, A. Sarkar, and A. Borics, "Universal properties and specificities of the β2-adrenergic receptor-g_s protein complex activation mechanism revealed by all-atom molecular dynamics simulations," *Int. J. Mol. Sci.* **22** (2021), 10.3390/ijms221910423.

[68]T. W. Schwartz, T. M. Frimurer, B. Holst, M. M. Rosenkilde, and C. E. Elling, "Molecular mechanism of 7tm receptor activation - a global toggle switch model," *Annu. Rev. Pharmacol. Toxicol.* **46** (2006), 10.1146/annurev.pharmtox.46.120604.141218.

[69]C. E. Elling, T. M. Frimurer, L. O. Gerlach, R. Jorgensen, B. Holst, and T. W. Schwartz, "Metal ion site engineering indicates a global toggle switch model for seven-transmembrane receptor activation," *J. Biol. Chem.* **281** (2006), 10.1074/jbc.M512510200.

[70]L. P. Picard, A. M. Schonegge, and M. Bouvier, "Structural insight into g protein-coupled receptor signaling efficacy and bias between gs and {beta-arrestin", *ACS Pharmacol. Transl. Sci.* **2** (2019), 10.1021/acsptsci.9b00012.

[71]D. Wang, Y. Yao, S. Wang, Y. Hou, L. Zhao, H. Wang, H. Chen, and J. Xu, "Structural insights into m1 muscarinic acetylcholine receptor signaling bias between g$\alpha\beta$ and β-arrestin through BRET assays and molecular docking," *Int. J. Mol. Sci.* **24** (2023), 10.3390/ijms24087356.

[72]E. Lyapina, E. Marin, A. Gusach, P. Orekhov, A. Gerasimov, A. Luginina, D. Vakhrameev, M. Ergasheva, M. Kovaleva, G. Khusainov, P. Khorn, M. Shevtsov, K. Kovalev, S. Bukhdruker, I. Okhrimenko, P. Popov, H. Hu,

U. Weierstall, W. Liu, Y. Cho, I. Gushchin, A. Rogachev, G. Bourenkov, S. Park, G. Park, H. J. Hyun, J. Park, V. Gordeliy, V. Borshchevskiy, A. Mishin, and V. Cherezov, "Structural basis for receptor selectivity and inverse agonism in S1P5 receptors," *Nat. Commun.* **13** (2022), 10.1038/s41467-022-32447-1.

[73]L. Yu, L. He, B. Gan, R. Ti, Q. Xiao, H. Hu, L. Zhu, S. Wang, and R. Ren, "Structural insights into sphingosine-1-phosphate receptor activation," *Proc. Natl. Acad. Sci. U. S. A.* **119** (2022), 10.1073/pnas.2117716119.

[74]D. J. Huggins, W. Sherman, and B. Tidor, "Rational approaches to improving selectivity in drug design," *J. Med. Chem.* **55** (2012), 10.1021/jm2010332.

[75]E. A. Wold and J. Zhou, "GPCR allosteric modulators: Mechanistic advantages and therapeutic applications," *Curr. Top. Med. Chem.* **18** (2019), 10.2174/1568026619999190101151837.

[76]P. E. G. F. Ibrahim, F. Zuccotto, U. Zachariae, I. Gilbert, and M. Bodkin, "Accurate prediction of dynamic protein–ligand binding using p-score ranking," *J. Comput. Chem.* **45**, 1762–1778 (2024).